

Weierstraß-Institut für Angewandte Analysis und Stochastik

im Forschungsverbund Berlin e.V.

Preprint

ISSN 0946 – 8633

R-matrix formalism for electron scattering in two dimensions

Paul N. Racec^{1,2}, Roxana Racec^{3,4}, Hagen Neidhardt¹

¹ Weierstraß-Institut für Angewandte Analysis und Stochastik, Mohrenstraße 39,
10117 Berlin, Germany,

E-Mail: racec@wias-berlin.de

E-Mail: neidhardt@wias-berlin.de

² National Institute of Materials Physics, PO Box MG-7, 077125 Bucharest
Magurele, Romania

³ Institut für Physik, Technische Universität Cottbus, Postfach 101344, 03013 Cot-
tbus, Germany,

E-Mail: roxana@physik.tu-cottbus.de

⁴ Faculty of Physics, University of Bucharest, PO Box MG-11, 077125 Bucharest
Magurele, Romania

submitted: October 29, 2009

No. 1452

Berlin 2009



2010 *Mathematics Subject Classification.* 35Q40, 35P25, 35B34.

2008 *Physics and Astronomy Classification Scheme.* 72.20.Dp, 73.40.-c, 73.63.-b.

Key words and phrases. Scattering, quantum transport, resonances, quantum dot, nanowire.

P. N. Racec acknowledges partial support from German Research Foundation (DFG) through SFB 787 "Semiconductor Nanophotonics: Materials, Models, Devices" under B4 and from the Romanian Ministry of Education and Research through the Program PNCDI2, Contract number 515/2008.

Edited by
Weierstraß-Institut für Angewandte Analysis und Stochastik (WIAS)
Mohrenstraße 39
10117 Berlin
Germany

Fax: + 49 30 2044975
E-Mail: preprint@wias-berlin.de
World Wide Web: <http://www.wias-berlin.de/>

Abstract

We investigate the scattering phenomena in two dimensions produced by a general finite-range nonseparable potential. This situation can appear either in a Cartesian geometry or in a heterostructure with cylindrical symmetry. Increasing the dimensionality of the scattering problem new processes as the scattering between conducting channels and the scattering from conducting to evanescent channels are allowed; for certain values of the energy, called resonance energy, the transmission through the scattering region changes dramatically in comparison with an one-dimensional problem. If the potential has an attractive character even the evanescent channels can be seen as dips of the total transmission. The multi-channel current scattering matrix is determined using its representation in terms of the R-matrix. The resonant transmission peaks are characterized quantitatively through the poles of the current scattering matrix. Detailed maps of the localization probability density sustain the physical interpretation of the resonances. Our formalism is applied to a quantum dot in a two-dimensional electron gas and to a conical quantum dot embedded inside a nanowire.

1 Introduction

There is a permanent requirement of shrinking the semiconductor devices in integrated circuits [1]. As feature sizes shrink into the nanometer scale regime, the device behavior becomes increasingly complicated since new physical phenomena at short distances occur and limitations in material properties are reached. In order to keep the good characteristics for transistors, new transistor architectures were developed progressively in the last decade.

Nowadays, there are developments of planar MOSFETs (metal oxide semiconductor field effect transistors) [2] as well as of gate-all-around (GAA) MOSFETs [3, 4, 5]. Both systems are also strongly related to more fundamental research structures developed in the last years, like in-plane-gate transistors [6], single-electron transistors [7], silicon on insulator planar double-gate transistors [8], non-planar double-gate FinFETs [9], non-planar trigate transistors [10], nanowire-based field-effect transistors (FET) [11], nanowire resonant tunneling diodes [12, 13], nanowire lasers [14], or nanowire qubits [15], whose maturity has still to be proven for industrial applications. Their structural complexity has also progressively increased, allowing for double-barrier structures [12, 13], or multiple core-shell layers [16, 14]. The material composition includes mainly III-V materials GaAs/AlGaAs [6, 7, 13], InAs/InP

[12], GaN/InGaN [14], but also group IV materials Si [4, 17], and Si/Ge [11, 15], predominant in the industry.

The transport phenomena in these mesoscopic devices go beyond the semi-classical limit, and a quantum mechanical description of the current and charge densities [18] is necessary. The most appropriate method for analyzing semiconductor devices with an active region in the nanometer scale and which are almost open (i.e. showing a strong coupling between the active region and contacts) is the scattering theory.

This paper is focused on systems for which the scattering process is a two-dimensional one. Such systems can appear either in a Cartesian geometry, like for devices tailored in a two-dimensional electron gas (2DEG) [6, 7], or in a cylindrical geometry, like for nanowire-based devices [3, 4, 5, 12, 13]. In these systems there is a strong confinement of the motion in one direction, called *transversal direction*, while the transport occurs in the other direction, called *longitudinal direction*. The scattering problem is a two-dimensional one because the scattering potential is nonseparable, and also the incoming electrons can choose different energy channels for transport which are mixed due to the scattering.

We present in this work a general method, valid within the effective mass approximation, for solving the two-dimensional (2D) Schrödinger equation with scattering boundary conditions. Its solutions are found using the scattering theory and the R-matrix formalism [19, 20, 21, 22, 23, 24, 25, 26, 27, 28, 29]. This method is a semi-analytical one, and it gives the scattering functions in each point inside and outside the scattering area and for each energy as a function of the solutions of the Wigner-Eisenbud problem. As known from the nuclear physics, the Wigner-Eisenbud problem is the eigenvalue problem of the Hamilton operator for the closed counterpart of the considered open quantum system [30]. The R-matrix formalism is not only numerically very efficient, but it is also suitable for higher dimensional nanostructures with complex geometry [20, 21, 22, 24, 25] and general nonseparable scattering potential [31, 32]. It can also deal with more than two terminals [26, 29].

Using the scattering functions we analyze further the transport properties of the open quantum structures, especially the conductance. Besides the low dimensionality of such systems, the open character is also an essential feature which controls the transport phenomena through the structure. When the quantum system becomes open, its eigenstates yield resonance states which do not have an infinite life time anymore and which are not strictly localized inside the quantum system. In this paper we identify the signature of the resonance in each conductance peak and study the influence of the nonseparable character of the potential on the resonances and on the conductance through the system.

An interesting effect in a multi-channel scattering problem is that as soon as the potential is not separable anymore, the channels get mixed. If furthermore the scattering potential is attractive, then it leads to unusual scattering properties, like resonant dips in the transmission coefficient just below the next channel minimum energy. As it was shown analytically for a δ scattering potential [33] and later on for a finite-range scattering potential [34, 35] the dips are due to quasi-bound-states

splitting off from a higher evanescent channel. So that evanescent channels can not be neglected when analyzing scattering in two- or three-dimensional quantum systems. These findings were recently confirmed numerically for a Gaussian-type scatterer [36] and also for a quantum dot or a quantum ring [37] embedded inside nanowires tailored in a two-dimensional electron gas (2DEG), or inside cylindrical nanowires [31]. The high resolution maps for the "near field" scattering wave functions presented in Refs. [36, 37, 31] show explicitly increased localization probability around the scatterer for energies of the quasi-bound states, in agreement with the resonant reflection or resonant back-scattering interpretation of these dips [33, 34]. The Cartesian and cylindrical geometries present different "selection rules" for the intersubband transmission [31].

2 Model

The electronic states in mesoscopic systems are easily described within the effective mass approximation whose validity requires that the envelope function $\Psi(E, \vec{r})$ must be slowly varying over dimensions comparable to the unit cell of the crystal [38].

In the spherical effective mass approximation, the envelope function associated to the energy E_{3D} satisfies a Schrödinger-type equation

$$\left[-\frac{\hbar^2}{2m^*} \Delta + V(\vec{r}) \right] \Psi(\vec{r}) = E_{3D} \Psi(\vec{r}). \quad (1)$$

The so-called *scattering potential* $V(\vec{r})$ contains the information about the confinement in the transversal direction, and inside the allowed area it is a sum of the heterojunction conduction band discontinuities, the electrostatic potential due to the ionized donors and acceptors, the self-consistent Hartree and exchange potentials due to free carriers, and external potentials. We use the symbol m^* to denote the effective mass of the electrons, while m denotes the magnetic quantum number.

For systems tailored in the 2DEG, the growth direction is chosen the z -direction, while the plane of the 2DEG is (x, y) . The wave function in the z -direction, $\xi(z)$, is taken as known (the simplest form is provided by Fang and Howard, [39]) so that the three-dimensional (3D) wave function can be written as

$$\Psi(E_{3D}; \vec{r}) = \xi(z) \psi(x, y). \quad (2)$$

The total energy

$$E_{3D} = E_{2DEG} + E, \quad (3)$$

where E_{2DEG} is the energy of the 2DEG level, and E is the energy associated with the motion in the plane of the 2DEG. The 3D Schrödinger type equation reduces to a two-dimensional Schrödinger equation [32]

$$\left[-\frac{\hbar^2}{2m^*} \left(\frac{\partial^2}{\partial x^2} + \frac{\partial^2}{\partial y^2} \right) + V(x, y) \right] \psi(x, y) = E \psi(x, y),$$

$$x \in (-\infty, \infty), y \in [-d_y, d_y]. \quad (4)$$

In the transversal direction the electron motion is limited at the interval $[-d_y, d_y]$ by a confining potential that we have considered as infinite. The nonseparable potential $V(x, y)$ varies strongly with the position only inside a small domain ($|x| \leq d_x$, $|y| \leq d_y$) which is usually called *scattering region* and is quasi-constant outside this domain.

For cylindrical nanowires, the azimuthal symmetry suggests to use cylindrical coordinates, with z axis along the nanowire [31]. As long as there are not split gates on the surface of the nanowire, the potential energy $V(\vec{r})$ is rotational invariant

$$V(\vec{r}) = V(r, z) \quad (5)$$

and nonseparable inside the scattering region. A scattering potential which does not explicitly depend on the azimuthal angle θ imposes the eigenfunctions of the orbital angular momentum operator L_z as solutions of Eq. (1)

$$\Psi_m(E_{3D}; r, \theta, z) = \zeta_m(\theta)\psi_m(r, z), \quad (6)$$

where

$$\zeta_m(\theta) = \frac{e^{im\theta}}{\sqrt{2\pi}}, \quad (7)$$

and $m = 0, \pm 1, \pm 2, \dots$ is the magnetic quantum number. This is an integer number due to the requirement that the function $e^{im\theta}$ should be single-valued. The functions $\psi_m(r, z)$ are determined from the equation

$$\left[-\frac{\hbar^2}{2m^*} \left(\frac{\partial^2}{\partial r^2} + \frac{1}{r} \frac{\partial}{\partial r} - \frac{m^2}{r^2} + \frac{\partial^2}{\partial z^2} \right) + V(r, z) \right] \psi_m(r, z) = E\psi_m(r, z),$$

$$z \in (-\infty, \infty), r \in [0, R], \quad (8)$$

where E denotes here the kinetic energy associated with the 3D motion of the electron inside the nanowire, $E = E_{3D}$. We have also considered an infinite potential outside the nanowire. In such a way, every magnetic quantum number m defines a *two-dimensional (2D) scattering problem*. Furthermore, these 2D scattering problems can be solved separately if the scattering potential is rotational invariant. How many of these problems have to be solved, depends on the specific physical quantity which has to be computed.

2.1 Scattering problem for two dimensions

We consider the following Schrödinger type equation in two dimensions, $(x_{\parallel}, x_{\perp})$, denoting generically the longitudinal and the transversal direction, respectively,

$$\left[-\frac{\hbar^2}{2m^*} \Delta_{x_{\parallel}, x_{\perp}} + V(x_{\parallel}, x_{\perp}) \right] \psi(E; x_{\parallel}, x_{\perp}) = E\psi(E; x_{\parallel}, x_{\perp}),$$

$$x_{\perp} \in \Omega, x_{\parallel} \in (-\infty, \infty). \quad (9)$$

One could consider here different effective masses in the longitudinal and transversal directions and also, for a layered heterostructure, a position-dependent effective mass. These effects can be incorporated in the formalism, but within this paper we neglect them for the simplicity of the exposure.

For the Cartesian geometry [32], in comparison with Eq. (4) we have

$$\begin{aligned} x_{\parallel} &= x, x_{\perp} = y, \Omega = [-d_y, d_y], \\ \Delta_{x_{\parallel}, x_{\perp}} &= \frac{\partial^2}{\partial x^2} + \frac{\partial^2}{\partial y^2}, \\ E &= E_{3D} - E_{2DEG}, \end{aligned} \quad (10)$$

while for the cylindrical geometry [31], in comparison with Eq. (8) we have

$$\begin{aligned} x_{\parallel} &= z, x_{\perp} = r, \Omega = [0, R], \\ \Delta_{x_{\parallel}, x_{\perp}} &= \frac{\partial^2}{\partial r^2} + \frac{1}{r} \frac{\partial}{\partial r} - \frac{m^2}{r^2} + \frac{\partial^2}{\partial z^2}, \\ E &= E_{3D}, \end{aligned} \quad (11)$$

which depends on the magnetic quantum number m .

The analogy between the both geometries appears more evident considering for the cylindrical geometry the unitary transformation $U : L^2([0, R] \times \mathbb{R}, r dr dz) \rightarrow L^2([0, R] \times \mathbb{R}, dr dz)$, with $Uf(r, z) = g(r, z) = \sqrt{r}f(r, z)$. The inverse transformation is $U^\dagger : L^2([0, R] \times \mathbb{R}, dr dz) \rightarrow L^2([0, R] \times \mathbb{R}, r dr dz)$, with $U^\dagger g(r, z) = f(r, z) = (1/\sqrt{r})g(r, z)$. In such a way, the Schrödinger operator becomes

$$\begin{aligned} \tilde{H}_{r,z} &= UH_{r,z}U^\dagger = U \left[-\frac{\hbar^2}{2m^*} \Delta_{z,r} + V(z, r) \right] U^\dagger \\ &= -\frac{\hbar^2}{2m^*} \left[\frac{\partial^2}{\partial r^2} - \frac{m^2 - 1/4}{r^2} + \frac{\partial^2}{\partial z^2} \right] + V(z, r). \end{aligned} \quad (12)$$

In turn, the term which contains $1/r^2$ and which is specific for the cylindrical geometry plays the role of a potential, and the Laplace operator appears as known for two dimensions in Cartesian coordinates. The current scattering matrix and the localization probability distribution density of an electron in a scattering state remain unchanged under this unitary transformation.

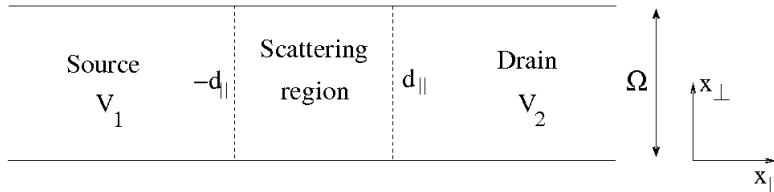


Figure 1: The generic geometry of the 2D scattering problem.

Due to the localized character of the scattering potential it is appropriate to solve Eq. (9) within the scattering theory. The potential energy which appears in Eq. (9) has generally two components:

$$V(x_{\parallel}, x_{\perp}) = V_{\perp}(x_{\perp}) + V_{scatt}(x_{\parallel}, x_{\perp}). \quad (13)$$

The first one, $V_{\perp}(x_{\perp})$, describes the lateral confinement of the electrons and is translation invariant along the parallel direction x_{\parallel} . We consider a hard wall potential

$$V_{\perp}(x_{\perp}) = \begin{cases} 0, & x_{\perp} \in \Omega \\ \infty, & x_{\perp} \notin \Omega \end{cases}, \quad (14)$$

which defines a quantum wire for the Cartesian geometry and a cylindrical nanowire for the second considered geometry. A parabolic wall like in Ref. [36, 37] may also be considered.

The scattering potential energy inside the nanowire, $V_{scatt}(x_{\parallel}, x_{\perp})$, has generally a nonseparable character in a domain of finite-range and is constant outside this domain. We consider here the nonseparable potential localized within the area $\Omega \times [-d_{\parallel}, d_{\parallel}]$, see Fig. 1,

$$V_{scatt}(x_{\parallel}, x_{\perp}) = \begin{cases} V_1, & x_{\perp} \in \Omega, x_{\parallel} < -d_{\parallel} \\ W(x_{\parallel}, x_{\perp}), & x_{\perp} \in \Omega, -d_{\parallel} \leq x_{\parallel} \leq d_{\parallel} \\ V_2, & x_{\perp} \in \Omega, x_{\parallel} > d_{\parallel} \end{cases}. \quad (15)$$

There are not material definitions for the interfaces $x_{\parallel} = \pm d_{\parallel}$. Usually, they are chosen inside the highly doped regions of the heterostructure characterized by a slowly variation of the potential in the longitudinal direction, practically by a constant potential. These regions play the role of the source and drain contacts.

2.2 Scattering states

In the asymptotic regions, $|x_{\parallel}| > d_{\parallel}$ i.e. source and drain contacts, the potential energy is separable in the transversal (i.e. confinement) and the longitudinal (i.e. transport) direction, i.e. $V(x_{\parallel}, x_{\perp}) = V_{\perp}(x_{\perp}) + V_s$, $s = 1, 2$, and Eq. (9) can be directly solved using the separation of variables method

$$\psi(E; x_{\parallel}, x_{\perp}) = \phi(x_{\perp})\varphi(x_{\parallel}). \quad (16)$$

The function $\phi(x_{\perp})$ satisfies the transversal equation

$$\left[-\frac{\hbar^2}{2m^*} \Delta_{x_{\perp}} + V_{\perp}(x_{\perp}) \right] \phi(x_{\perp}) = E_{\perp} \phi(x_{\perp}), \quad x_{\perp} \in \Omega \quad (17)$$

where

$$\Delta_{x_{\perp}} = \begin{cases} \frac{d^2}{dy^2}, & \text{Cartesian geometry} \\ \frac{d^2}{dr^2} + \frac{1}{r} \frac{d}{dr} - \frac{m^2}{r^2}, & \text{cylindrical geometry} \end{cases}. \quad (18)$$

The hard wall confinement potential requires Dirichlet boundary condition at the boundaries $\partial\Omega$ of the interval Ω , $\phi(\partial\Omega) = 0$. As a remark, for the cylindrical geometry, the boundary $r = 0$ is an artificial one introduced in order to use the cylindrical symmetry. At this boundary it is sufficient that $\phi(x_\perp)$ remains finite.

Due to the electron confinement in the transversal direction x_\perp the solutions of Eq. (17) define the *transversal modes*, $\phi_n(x_\perp)$, with the corresponding transversal energies $E_{\perp n}$, $n \geq 1$. The eigenfunctions $\phi_n(x_\perp)$ depend on the geometry (Cartesian or cylindrical) and on the confinement potential. In the case of a hard wall confinement, the transversal modes are given for the Cartesian geometry by sine functions [32], while for the cylindrical geometry they are expressed in terms of the Bessel functions of the first kind [31]. The transversal modes form an orthonormal and complete system of functions.

The function $\varphi(x_\parallel)$ satisfies the one-dimensional Schrödinger type equation called longitudinal equation

$$\left[-\frac{\hbar^2}{2m^*} \frac{d^2}{dx_\parallel^2} + V_s \right] \varphi(x_\parallel) = (E - E_\perp) \varphi(x_\parallel), \quad x_\parallel \in (-\infty, -d_\parallel) \cup (d_\parallel, \infty), \quad (19)$$

where $s = 1$ stays for the source contact ($x_\parallel < -d_\parallel$) and $s = 2$ for the drain contact ($x_\parallel > d_\parallel$). In the case of different effective masses in transversal and longitudinal direction, one can use the corresponding effective mass in each of the above equations.

Every transversal mode together with the associated motion on the transport direction defines a *scattering channel* on each side of the scattering area. The scattering channels are indexed by (sn) , $n \geq 1$, $s = 1, 2$ for each E . In contradistinction to the Cartesian geometry, in the case of a cylindrical geometry there is a set of 2D scattering problems, indexed by the magnetic quantum number m , that have to be solved. Consequently the scattering channels should be also indexed by m . For simplicity we omit the index m in this section, but we keep in mind that we solve here a 2D scattering problem and obtain the scattering functions for a fix value of m .

If the total energy E and the lateral eigenenergy $E_{\perp n}$ are fixed, there are at most two linearly independent solutions of Eq. (19). In the asymptotic region they are given as a linear combination of exponential functions

$$\varphi_{sn}(x_\parallel) = \begin{cases} A_s e^{ik_{1n}x_\parallel} + B_s e^{-ik_{1n}x_\parallel}, & x_\parallel < -d_\parallel \\ C_s e^{ik_{2n}x_\parallel} + D_s e^{-ik_{2n}x_\parallel}, & x_\parallel > d_\parallel \end{cases} \quad (20)$$

where A_s , B_s , C_s and D_s are complex coefficients depending on n and E for each value of $s = 1, 2$. The wave vector is defined for each scattering channel (sn) as

$$k_{sn}(E) = k_0 \sqrt{(E - E_{\perp n} - V_s)/u_0}, \quad (21)$$

where $k_0 = \pi/2d_\parallel$ and $u_0 = \hbar^2 k_0^2 / 2m^*$. In the case of the conducting or open channels

$$E - E_{\perp n} - V_s \geq 0, \quad (22)$$

k_{sn} are positive real numbers and correspond to propagating plane-waves. For the evanescent or closed channels

$$E - E_{\perp n} - V_s < 0, \quad (23)$$

k_{sn} are given from the first branch of the complex square root function, $k_{sn} = i|k_{sn}|$, and describe exponentially decaying functions away from the scattering region. Thus, the number of the conducting channels, $N_s(E)$, $s = 1, 2$, is a function of energy, and for a fixed energy E this is the largest value of n , which satisfies the inequality (22) for given values of s .

Each conducting channel corresponds to one degree of freedom for the electron motion through the system and, consequently, there exists only one independent solution of Eq. (9) for a fixed channel (sn) associated with the energy E , $\psi_n^{(s)}(E; x_{\parallel}, x_{\perp})$. For describing further the transport phenomena in the frame of the scattering theory it is convenient to consider this solution as a *scattering state*, i.e. as a sum of an incoming component on the channel (sn) and a linear combination of outgoing components on each scattering channel. One can write the scattering wave functions in a compact form [32]

$$\begin{aligned} \psi_n^{(s)}(E; x_{\parallel}, x_{\perp}) &= \frac{\theta(N_s(E) - n)}{\sqrt{2\pi}} \\ &\times \begin{cases} \delta_{s1} e^{ik_{1n}(x_{\parallel} + d_{\parallel})} \phi_n(x_{\perp}) + \sum_{n'=1}^{\infty} S_{1n',sn}(E) e^{-ik_{1n'}(x_{\parallel} + d_{\parallel})} \phi_{n'}(x_{\perp}), & x_{\parallel} < -d_{\parallel} \\ \delta_{s2} e^{-ik_{2n'}(x_{\parallel} - d_{\parallel})} \phi_n(x_{\perp}) + \sum_{n'=1}^{\infty} S_{2n',sn}(E) e^{ik_{2n'}(x_{\parallel} - d_{\parallel})} \phi_{n'}(x_{\perp}), & x_{\parallel} > d_{\parallel} \end{cases} \quad (24) \end{aligned}$$

The step function θ in the above expressions, with $\theta(x \geq 0) = 1$ and $\theta(x < 0) = 0$, assures that the scattering functions are defined only for the conducting channels. Writing explicitly the position of the interfaces $\pm d_{\parallel}$ at the exponent has advantages for the analytical treatment of the scattering problem [22, 40]. As it is discussed in Refs. [26, 31], it is necessary to consider the sum until infinity in the second term of the above expression, in order to keep the mathematical completeness of the transversal channels.

The physical interpretation of the expressions (24) is that, due to the nonseparable character of the scattering potential, a plane-wave incident onto the scattering domain is reflected on every channel - open or closed for transport - on the same side of the system and transmitted on every channel - open or closed for transport - on the other side. The reflection and transmission amplitudes are described by the complex coefficients $S_{sn',sn}$ and $S_{s'n',sn}$ with $s \neq s'$, respectively, and all of them should be nonzero. These coefficients define a matrix with $N_1(E) + N_2(E)$ infinite columns. For an elegant solution of the scattering problem we extend $S(E)$ to an infinite square matrix and set at zero the matrix elements without physical meaning, $S_{s'n',sn}(E) = 0$, $n > N_s(E)$, $s = 1, 2$. In this way we define the *wave transmission matrix* or *wave-function amplitudes matrix* [33]. It is also called *generalized scattering matrix* [41]. This is not the well-known scattering matrix (current transmission

matrix) whose unitarity reflects the current conservation. The generalized scattering matrix is a non-unitary matrix, which has the advantage that it allows for a description of the scattering processes not only in the asymptotic region but also inside the scattering area.

The three-dimensional scattering states, solutions of Eq. (1) can be now written as

$$\Psi_n^{(s)}(E; x_{\parallel}, x_{\perp}, x_3) = \omega(x_3)\psi_n^{(s)}(E; x_{\parallel}, x_{\perp}), \quad (25)$$

where $\omega(x_3)$ stays for $\xi(z)$ in the case of the Cartesian geometry and for $\zeta_m(\theta)$ in the case of the cylindrical geometry. Being eigenfunctions of an open system, the scattering states are ortho-normalized in the general sense [27]

$$\int_{\Omega} d\Omega \int_{-\infty}^{\infty} dx_{\parallel} \psi_n^{(s)}(E; x_{\parallel}, x_{\perp}) \psi_{n'}^{(s')} (E'; x_{\parallel}, x_{\perp})^* = \delta_{ss'} \delta_{nn'} \frac{\delta(E - E')}{g_{sn}(E)}, \quad (26)$$

where $g_{sn}(E) = m^*/[\hbar^2 k_{sn}(E)]$ is the 1D density of states. We have to mention that for the Cartesian coordinates [32], the measures are $d\Omega = dy$, $dx_{\parallel} = dx$, while for the cylindrical geometry [31] they are $d\Omega = r dr$, $dx_{\parallel} = dz$.

2.3 R-matrix formalism for two dimensions

The scattering functions inside the scattering region are determined using the R-matrix formalism, i.e. they are expressed in terms of the eigenfunctions corresponding to the closed counterpart of the scattering problem [19, 20, 21, 22, 23, 24, 25, 26, 29]. In our opinion this is a more appropriate method than the common mode space approach which implies the expansion of the scattering functions inside the scattering area in the basis of the transversal modes $\phi_n(x_{\perp})$. As it is shown in Refs. [35, 42] the mode space approach has limitations for structures with abrupt changes in the potential or sudden spatial variations in the widths of the wire; it breaks even down for coupling operators that are not scalar potentials, like in the case of an external magnetic field. In the R-matrix formalism the used basis contains all the information about the scattering potential, and this type of difficulties can not appear.

Thus, the scattering functions inside the scattering region are given as

$$\psi_n^{(s)}(E; x_{\parallel}, x_{\perp}) = \sum_{l=1}^{\infty} a_{ln}^{(s)}(E) \chi_l(x_{\parallel}, x_{\perp}), \quad (27)$$

with $x_{\perp} \in \Omega$ and $x_{\parallel} \in [-d_{\parallel}, d_{\parallel}]$.

The so-called *Wigner-Eisenbud functions*, $\chi_l(x_{\parallel}, x_{\perp})$, firstly used in the nuclear physics [30, 43], satisfy the same equation as $\psi_n^{(s)}(x_{\parallel}, x_{\perp})$, Eq. (9), but with different boundary conditions in the transport direction. Since the scattering function $\psi_n^{(s)}(x_{\parallel}, x_{\perp})$ satisfies energy dependent boundary conditions derived from Eq. (24) due to the continuity of the scattering function and its derivative at $x_{\parallel} = \pm d_{\parallel}$, the

Wigner-Eisenbud function $\chi_l(x_{\parallel}, x_{\perp})$ has to satisfy Neumann boundary conditions at the interfaces between the scattering region and leads

$$\left. \frac{\partial \chi_l}{\partial x_{\parallel}} \right|_{x_{\parallel}=\pm d_{\parallel}} = 0, \quad l \geq 1. \quad (28)$$

The hard wall confinement potential requires Dirichlet boundary condition at $\partial\Omega$ also for the Wigner-Eisenbud functions, $\chi_l(\partial\Omega, x_{\parallel}) = 0$. As already mentioned for the scattering states, for the cylindrical geometry it is sufficient that the Wigner-Eisenbud function remains finite at $r = 0$. The functions χ_l , $l \geq 1$, build a basis which verifies the orthogonality relation

$$\int_{\Omega} d\Omega \int_{-d_{\parallel}}^{d_{\parallel}} dx_{\parallel} \chi_l(x_{\perp}, x_{\parallel}) \chi_{l'}(x_{\perp}, x_{\parallel}) = \delta_{ll'} \quad (29)$$

and the closure relation

$$\sum_{l=1}^{\infty} \chi_l(x_{\perp}, x_{\parallel}) \chi_l(x'_{\perp}, x'_{\parallel}) = \delta(x_{\perp} - x'_{\perp}) \delta(x_{\parallel} - x'_{\parallel}). \quad (30)$$

Note that for the cylindrical geometry $\delta(x_{\perp} - x'_{\perp})$ in the relation (30) means $\delta(r - r')/r$. The corresponding eigenenergies to χ_l are denoted by E_l and are called *Wigner-Eisenbud energies*. Since the Wigner-Eisenbud problem is defined on a closed volume with self-adjoint boundary conditions, the eigenfunctions χ_l and the eigenenergies E_l can be chosen as real quantities. The Wigner-Eisenbud problem is, thus, the closed counterpart of the scattering problem.

In the case of the one-dimensional system without spherical symmetry, it was recently proven mathematically rigorous that the R-matrix formalism allows for a proper expansion of the scattering matrix on the real energy axis [28]. In this section we present an extension of the R-matrix formalism for 2D scattering problem.

To calculate the expansion coefficients $a_{ln}^{(s)}(E)$ we multiply Eq. (9) by $\chi_l(x_{\parallel}, x_{\perp})$ and the equation satisfied by the Wigner-Eisenbud functions by $\psi_n^{(s)}(E; x_{\parallel}, x_{\perp})$. The difference between the resulting equations is integrated over $\Omega \times [-d_{\parallel}, d_{\parallel}]$, with the corresponding measures, and one obtains on the right-hand side the coefficient $a_{ln}^{(s)}(E)$. After using the Green's theorem and the boundary conditions one finds $a_{ln}^{(s)}(E)$ and feeds in it into Eq. (27). So, *the scattering functions inside the scattering region* ($x_{\parallel} \in [-d_{\parallel}, d_{\parallel}]$, $x_{\perp} \in \Omega$) are obtained in terms of their derivatives at the edges of this domain,

$$\psi_n^{(s)}(E; x_{\parallel}, x_{\perp}) = \frac{1}{k_0} \int_{\Omega} dx'_{\perp} \left[R(E; -d_{\parallel}, x'_{\perp}, x_{\parallel}, x_{\perp}) \left. \frac{\partial \psi_n^{(s)}(E; x'_{\parallel}, x'_{\perp})}{\partial x'_{\parallel}} \right|_{x'_{\parallel}=-d_{\parallel}} - R(E; d_{\parallel}, x'_{\perp}, x_{\parallel}, x_{\perp}) \left. \frac{\partial \psi_n^{(s)}(E; x'_{\parallel}, x'_{\perp})}{\partial x'_{\parallel}} \right|_{x'_{\parallel}=d_{\parallel}} \right], \quad (31)$$

where the R -function is defined as

$$R(E; x_{\parallel}, x_{\perp}, x'_{\parallel}, x'_{\perp},) \equiv \frac{u_0}{k_0} \sum_{l=1}^{\infty} \frac{\chi_l(x_{\parallel}, x_{\perp}) \chi_l(x'_{\parallel}, x'_{\perp})}{E - E_l}. \quad (32)$$

The functions $\partial\psi_n^{(s)}/\partial x_{\parallel}$ at $x_{\parallel} = \pm d_{\parallel}$ are calculated from the asymptotic form (24) based on the continuity conditions for the derivatives of the scattering functions on the interfaces between the scattering region and leads.

With these results the scattering functions inside the scattering domain are expressed in terms of the wave transmission matrix \mathbf{S}

$$\vec{\Psi}(E; x_{\parallel}, x_{\perp}) = \frac{i}{\sqrt{2\pi}} \mathbf{\Theta}(E) [\mathbf{1} - \mathbf{S}^T(E)] \mathbf{K}(E) \vec{R}(E; x_{\parallel}, x_{\perp}), \quad (33)$$

where the component (sn) of the vector $\vec{\Psi}$ is the scattering function $\psi_n^{(s)}(E; x_{\parallel}, x_{\perp})$, $n \geq 1$, $s = 1, 2$ and \mathbf{S}^T denotes the matrix transpose. The diagonal matrix \mathbf{K} has on its diagonal the wave vectors (21) of each scattering channel

$$\mathbf{K}_{sn,s'n'}(E) = \frac{k_{sn}(E)}{k_0} \delta_{nn'} \delta_{ss'}, \quad (34)$$

$n, n' \geq 1$, $s, s' = 1, 2$, and the vector $\vec{R}(E; x_{\parallel}, x_{\perp})$ is given as

$$\vec{R}(E; x_{\parallel}, x_{\perp}) = \frac{u_0}{\sqrt{k_0}} \sum_{l=1}^{\infty} \frac{\chi_l(x_{\parallel}, x_{\perp}) \vec{\chi}_l}{E - E_l}, \quad (35)$$

where $\vec{\chi}_l$ has the components

$$(\vec{\chi}_l)_{sn} = \frac{1}{\sqrt{k_0}} \int_{\Omega} \chi_l(x_{\perp}, (-1)^s d_{\parallel}) \phi_n(x_{\perp}) d\Omega, \quad (36)$$

$n \geq 1$, $s = 1, 2$. The diagonal *Theta*-matrix, $\mathbf{\Theta}_{sn,s'n'}(E) = \theta(N_s(E) - n) \delta_{ss'} \delta_{nn'}$, $n \geq 1$, $s = 1, 2$, assures non-zero values only for the scattering functions corresponding to the conducting channels.

Using further the continuity of the scattering functions on the surface of the scattering area and expanding $\vec{R}(E; \pm d_{\parallel}, x_{\perp})$ in the basis $\{\phi_n(x_{\perp})\}_{n \geq 1}$ we find the relation between the matrixes \mathbf{S} and \mathbf{R}

$$\mathbf{S}(E) = [\mathbf{1} - 2(\mathbf{1} + i\mathbf{R}(E)\mathbf{K}(E))^{-1}] \mathbf{\Theta}(E), \quad (37)$$

with the R -matrix given by means of a dyadic product

$$\mathbf{R}(E) = u_0 \sum_{l=1}^{\infty} \frac{\vec{\chi}_l \vec{\chi}_l^T}{E - E_l}. \quad (38)$$

According to the above relation, \mathbf{R} is an infinite-dimensional symmetrical real matrix and its elements defined by Eq. (38) are dimensionless. The above form allows for a very efficient numerical implementation for computing the R -matrix.

The expression (37) of the S -matrix in terms of the R -matrix is the key relation for solving 2D scattering problems using only the eigenfunctions and the eigenenergies of the closed quantum system. They contain the full information about the scattering potential and carry it over to the R -matrix. The matrix \mathbf{K} characterizes the contacts and can be constructed using only the information about the potential in these regions. On the base of Eq. (37) the wave transmission matrix is calculated and after that the scattering functions in each point of the system are obtained using Eqs. (24) and (33). Further on, each transport property of the open quantum system can be derived from the scattering function in terms of the scattering matrix.

2.4 Reflection and transmission coefficients

Using the density current operator

$$\vec{j}(\vec{r}) = \frac{\hbar}{2im^*} \left(\Psi(\vec{r}) \nabla \Psi(\vec{r})^* - \Psi(\vec{r})^* \nabla \Psi(\vec{r}) \right), \quad (39)$$

one can define, as usually, the transmission and reflection probabilities [44]. Here $\Psi(\vec{r})^*$ denotes the complex conjugate of the scattering wave function (25).

The transversal component of the density current $j_{\perp}(x_{\perp}, x_{\parallel}, x_3)$ is zero in leads, because $\phi_n(x_{\perp})$ are real functions. The component x_3 of the incident density current is also zero, either due to the confinement in the third direction, like in Cartesian geometry [32], or due to the symmetry reasons like for the cylindrical geometry [31]. What remains is the longitudinal component of the particle density current $j_{\parallel}(x_{\perp}, x_{\parallel}, x_3)$, which provides after the integration over the cross section of the lead with the corresponding measure, $d\Omega$, the very well-known relations for the transmission and reflection probabilities. The probability for an electron incident from the source, $s = 1$, on the channel n to be reflected back into the source on the channel n' is

$$R_{nn'}^{(1)} = \frac{k_{1n'}}{k_{1n}} |S_{1n,1n'}^T|^2, \quad (40)$$

and the probability to be transmitted into the drain, $s = 2$, on the channel n' is

$$T_{nn'}^{(1)} = \frac{k_{2n'}}{k_{1n}} |S_{1n,2n'}^T|^2. \quad (41)$$

The reflection and transmission probabilities for the evanescent (closed) channels are zero. The total transmission and reflection coefficients for an electron incident from reservoir $s = 1$ are defined as

$$T^{(1)} = \sum_{n,n'} T_{nn'}^{(1)}, \quad R^{(1)} = \sum_{n,n'} R_{nn'}^{(1)}. \quad (42)$$

More detailed properties of the many-channel tunneling and reflection probabilities are given in Ref. [44], but note that our indexes are interchanged with respect to the definitions used there.

2.5 Current scattering matrix

Further, we define the energy dependent *current scattering matrix* as

$$\tilde{\mathbf{S}}(E) = \mathbf{K}^{1/2}(E)\mathbf{\Theta}(E)\mathbf{S}(E)\mathbf{K}^{-1/2}(E), \quad (43)$$

so that its elements give directly the reflection and transmission probabilities

$$\begin{aligned} |\tilde{S}_{1n',1n}(E)|^2 &= R_{nn'}^{(1)}(E), & |\tilde{S}_{2n',2n}(E)|^2 &= R_{nn'}^{(2)}(E), \\ |\tilde{S}_{2n',1n}(E)|^2 &= T_{nn'}^{(1)}(E), & |\tilde{S}_{1n',2n}(E)|^2 &= T_{nn'}^{(2)}(E). \end{aligned} \quad (44)$$

The diagonal Θ -matrix assures that the matrix elements of $\tilde{\mathbf{S}}$ are nonzero only for the conducting channels, for which the transmitted flux is nonzero. Using the R -matrix representation of \mathbf{S} , Eq. (37), we find from the above relation

$$\tilde{\mathbf{S}}(E) = \mathbf{\Theta}(E) \left[\mathbf{1} - 2(\mathbf{1} + i\mathbf{\Omega}(E))^{-1} \right] \mathbf{\Theta}(E), \quad (45)$$

with the infinite dimensional matrix $\mathbf{\Omega}$

$$\mathbf{\Omega}(E) = \mathbf{K}^{1/2}(E)\mathbf{R}(E)\mathbf{K}^{1/2}(E) = u_0 \sum_{l=1}^{\infty} \frac{\vec{\alpha}_l \vec{\alpha}_l^T}{E - E_l} \quad (46)$$

and the column vector

$$\vec{\alpha}_l(E) = \mathbf{K}^{1/2}(E) \vec{\chi}_l, \quad (47)$$

with $l \geq 1$.

Further we express the total tunneling coefficient in terms of the current transmission matrix,

$$T(E) = \text{Tr}[\boldsymbol{\sigma}(E)\boldsymbol{\sigma}^\dagger(E)], \quad (48)$$

where $\boldsymbol{\sigma}$ denotes the part of $\tilde{\mathbf{S}}$ which contains the transmission, $\sigma_{nn'}(E) = \tilde{S}_{2n',1n}(E)$, $n = \overline{1, N_1(E)}$ and $n' = \overline{1, N_2(E)}$.

According to the definition (46) the matrix $\mathbf{\Omega}$ is a symmetrical one, $\mathbf{\Omega} = \mathbf{\Omega}^T$, and from Eq. (45) it follows that $\tilde{\mathbf{S}}$ also has this property, $\tilde{\mathbf{S}} = \tilde{\mathbf{S}}^T$. On this basis one can demonstrate that the tunneling coefficient characterizes one pair of open channels irrespective of the origin of the incident flux $T_{nn'}^{(1)} = |\tilde{S}_{2n',1n}|^2 = |\tilde{S}_{1n,2n'}|^2 = T_{n'n}^{(2)}$. This is a well-known property of the transmission through a scattering system and it shows that the current scattering matrix used here is properly defined. The restriction of \tilde{S} -matrix to the open channels is the well known current scattering matrix [20, 22, 23], commonly used in the Landauer-Büttiker formalism. For a given energy E this is a $(N_1 + N_2) \times (N_1 + N_2)$ matrix which has to satisfy the unitarity condition, according to the flux conservation.

In the numerical computations, the matrixes \mathbf{S} , \mathbf{R} , $\mathbf{\Omega}$, $\tilde{\mathbf{S}}$ and $\mathbf{\Theta}$ have the dimension $2N \times 2N$, and the vectors $\vec{\chi}_l$, $\vec{\alpha}_l(E)$ have $2N$ components, where N is the number of scattering channels (open and closed) taken numerically into account. The number of the Wigner-Eisenbud functions and energies computed numerically establishes the maximum value for the index l .

2.6 Resonances

The relation (45) is the starting point for a resonance theory of the transmission through a structure with a scattering region [22, 32]. The singularities of the current scattering matrix $\tilde{\mathbf{S}}$ which satisfy the equation

$$\det [\mathbf{1} + i\mathbf{\Omega}(E)] = 0 \quad (49)$$

are usually classified as bound states and resonances. The bound states are characterized by real negative energies while the resonance energies, $\bar{E}_{0l} = E_{0l} - i\Gamma_l/2$, $l \geq 1$, lie in the complex energy plane below the real positive axis according to the causality [45]. The scattering matrix $\tilde{\mathbf{S}}$ and consequently the total transmission $T(E)$ are defined only for energies in the continuum spectrum (E real positive) of the scattering problem and they are analytical functions over the whole domain. Although they have no singularities in the definition domain, their energy dependence is determined by the resonances, especially by those ones which lie in the vicinity of the real axis. In the resonance domain, i.e. inside a circle of radius Γ_l around \bar{E}_{0l} , the elements of the current scattering matrix $\tilde{\mathbf{S}}$ vary strongly with the energy. In turn, $T(E)$ has also an important variation for the real energies included in the resonance domain. Thus the resonances appear usually as peaks in the tunneling coefficient and can be directly seen in the transport properties of the structure. While in the case of a 1D scattering potential the peaks are light asymmetric maxima [22], for a 2D scattering potential the peak shapes cover all ranges of the Fano lines, from asymmetric maxima through "S-type" Fano lines up to antiresonances. These profiles have been already seen experimentally for example in the conductance of a single-electron transistor [7]. In the next section we demonstrate that the two-dimensional character of the scattering potential and the strong coupling of the quantum system to the contacts allow for the transmission profiles which are far from Breit-Wigner lines.

The representation of the \tilde{S} -matrix in terms of $\mathbf{\Omega}$, Eq. (45) allows for an efficient numerical procedure to determine its poles and the resonances. When the quantum system, for example a quantum dot, is coupled to the contacts it becomes open, and the real eigenenergies of the closed problem, E_l , migrate in the lower part of the complex energy plane, becoming resonant energies, $\bar{E}_{0l} = E_{0l} - i\Gamma_l/2$, $l \geq 1$. On the base of this correspondence we fix an energy E_λ of the isolated dot and determine the resonance energy $\bar{E}_{0\lambda}$ as a solution of Eq. (49) in the complex energy plane. The matrix $\mathbf{\Omega}$ contains contributions from all Wigner-Eisenbud functions and energies, i.e. χ_l and E_l , and from all scattering channels, i.e. all matrix elements of \mathbf{K} . Thus the resonance energy $\bar{E}_{0\lambda}$ can strongly differ from E_λ , and only in the case of a very low coupling of the dot to the contacts the eigenenergies of the isolated system, E_λ , can properly approximate the real part of the resonance energy.

The resonance theory presented above is general and can be applied to a variety of structures with a 2D scattering potential, regardless if the geometry of the system is Cartesian or cylindrical. The information about the geometry is contained only in the Wigner-Eisenbud functions and energies. After solving the eigenvalue problem

of the closed counterpart of the scattering system one can construct the scattering matrix and analyze it without bearing in mind the geometry of the system.

The expression (45) of the \tilde{S} -matrix shows that all matrix elements of $\tilde{\mathbf{S}}$ are singular at the resonance energy. That means that all transmission coefficients $T_{nn'}$ between different scattering channels have a similar dependence on energy around a resonance, and it is enough to analyze the total transmission which is a sum of them in order to characterize the resonance.

3 Model systems

Further we analyze the total tunneling coefficient $T(E)$ for a large energy interval in the case of a quantum dot isolated inside of a 2DEG (*Cartesian geometry*) and in the case of a conical quantum dot in a cylindrical nanowire (*cylindrical geometry*). The transmission peaks are directly connected to the resonances and they have different profiles depending on the coupling strength between the quantum system and contacts, but also between resonances.

3.1 Quantum dot in two-dimensional electron gas

We consider here a quite simple dot, a square dot, isolated inside a quantum wire by the constant barriers V_0 as seen in Fig. 2. The smaller barriers V_{b1} and V_{b2} characterize the coupling between the quantum dot and contacts, and the strength of this coupling can be varied individually. Although our model allows for an arbitrary form of the potential, we have chosen this square dot in order to compare the scattering functions at the resonant energies with the eigenfunctions of an isolated dot ($V_0, V_{b1}, V_{b2} \rightarrow \infty$).

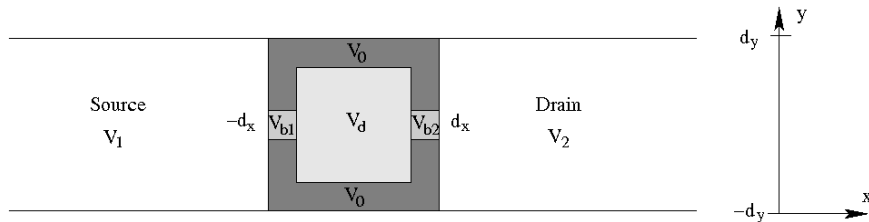


Figure 2: Potential energy in the 2D quantum wire: constant potential energy in the source and drain contacts, $V_1 \simeq V_2$, and position-dependent potential energy in the dot-region. The quantum dot is isolated inside the quantum wire by the barrier with the height V_0 . The coupling between dot and contacts is set by the potential energy in the aperture regions, V_{b1} and V_{b2} . The electrons inside the dot experience the potential energy V_d .

For the numerical calculations we have set $d_x = d_y = 50$ nm, and the width of all

barrier 20 nm. Thus the region where the electrons are localized is about 60×60 nm. The barrier which isolates the quantum dot inside the quantum wire has been taken as $V_0 = 0.4$ eV, and the potential energy in the aperture regions $V_{b1} = V_{b2} = 0.005$ eV. In the source and drain contacts the potential energy has been considered as the energy reference, $V_1 = V_2 = 0$ eV. The Fermi energy of the electrons has been taken as $E_F = 12$ meV. For this quantum dot there are four open channels, $N_1(E_F) = N_2(E_F) = 4$, and the closed channels do not have a significant contribution to the conductance.

The quantum dot described above is strongly coupled to the source and drain contacts because the potential energy in the aperture regions lies under the Fermi energy. For explaining the transport phenomena through the dot it is necessary to take properly into account the open character of the system and to analyze the transport properties in terms of the resonances. The eigenstates which characterize the closed counterpart of the open dot have an infinite life time and can not explain the broaden peaks which are experimentally measured in the conductance of an open quantum dot [7].

The resonance energies of the considered dot, solutions of Eq. (49), are presented in Fig. 3. For comparison, the Wigner-Eisenbud energies, i.e. the eigenenergies of the corresponding isolated dot are also given. Due to the coupling of the quantum dot to the contacts the resonance energies migrate in the lower part of the complex energy plane and have different widths. There are very narrow resonances, which can be associated with the modes of the dot that are not so strongly coupled to the contacts, and broad resonances, which describe modes strongly perturbed by the interaction with the reservoirs. For a better understanding of the resonance modes we will examine the localization probability distribution density of the electrons for the energies given by the real part of the resonance energy \bar{E}_{0l} .

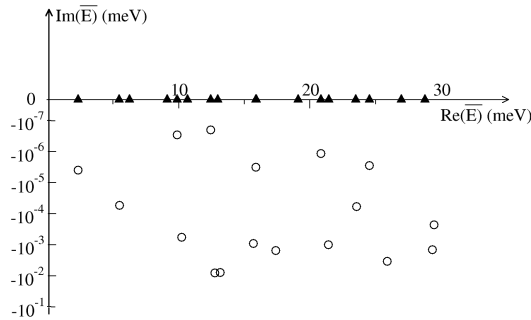


Figure 3: Resonance energies \bar{E}_{0l} (empty circles) of the open quantum dot given in Fig. 2 and the real eigenenergies E_l (filled triangles) of the isolated counterpart of the considered quantum dot.

The potential energy felt by the electrons inside the dot is V_d . This energy can be modified continuously by varying the voltage of a plunger gate [20, 22, 23], and the conductance through the dot is measured as a function of V_d . In the linear

regime experiments, i.e. small source drain biases, and for very low temperatures the conductance G can be directly connected to the total tunneling coefficient at the Fermi energy [7, 22, 32],

$$G(V_d) = \frac{2e^2}{h} T(E_F; V_d). \quad (50)$$

In the above relation the potential energy V_d appears as a parameter in the expression of the total tunneling coefficient. A new value of V_d means a new scattering potential and a new scattering matrix. But there is no analytic dependence of T on V_d , so that the scattering matrix and after that the conductance have been numerically computed for each value of V_d . In Figs. 4 and 5 the conductance is plotted as a function of $E_F - V_d$. This fact has the great advantage that the position of the maxima in conductance are given with respect to the bottom of the quantum well, and in this way a direct comparison with an infinite quantum well is possible. There are narrow and broad peaks in the conductance and in order to understand why they have different profiles we have also plotted the electron probability distribution density $P_n(x, y) = |\psi_n^{(1)}(E; x, y)|^2$ for $E = E_F$ and $V_d = V_{0l}$, for the eight peaks considered here, $l = \overline{1, 8}$. In principle the potential energy V_{0l} is associated with the maximum of the conductance peak, but the conductance curve shows also a "S-type" Fano line, and a rigorous method to fix V_{0l} is necessary.

Using the R-matrix representation of the S-matrix, Eq. (45) we can provide an approximative relation for $T(E_F, V_d)$ around a resonance

$$T(E_F, V_d) = T(E_F, V_{0l} + \delta V) \simeq T(E_F - \delta V, V_{0l}) \quad (51)$$

where V_{0l} is the value of V_d for which the real part of the resonance energy ($\bar{E}_{0l} = E_{0l} - i\Gamma_l/2$) matches the Fermi energy, $E_{0l} = E_F$, and δV is a small variation with values in the interval $(-\Gamma_l, \Gamma_l)$. For a detailed discussion of this approach see Ref. [22], Appendix A. The expression (51) of the total tunneling coefficient allows for a direct connection to the resonances. We can simultaneously plot the conductance as a function of $E_F - \delta V$, $\delta V \in (-\Gamma_l, \Gamma_l)$ and the resonances with the real energies in the interval $(E_F - \Gamma_l, E_F + \Gamma_l)$. These plots are given in Figs. 4 and 5. The dashed vertical lines correspond in each picture to $\delta V = 0$, i.e. $V_d = V_{0l}$ in the plots in the middle part and $E = E_F$ in the plots in the lower part. From the simultaneous analysis of these graphics it is evident that we can associate each peak in the conductance with a resonance l . At the resonance energy the electrons show a strong localization in the dot region, shown in the upper part of the figures. A narrow peak corresponds to a resonance energy with a very small imaginary part and to a resonance state that is almost decoupled from the contacts, i.e the electron probability distribution density is nearly zero in the aperture regions. These are the resonances denoted by (3), (4), (6) and (8) in Figs. 4 and 5. The other peaks are broaden and they correspond to resonances with a larger imaginary part and to states which are strongly coupled to the contacts. Generally, the peaks for which the resonance states have a maximum at $y = 0$ couple strongly to the contacts and become broaden. These are the peaks (1), (2), (5) and (7) in Figs. 4 and 5.

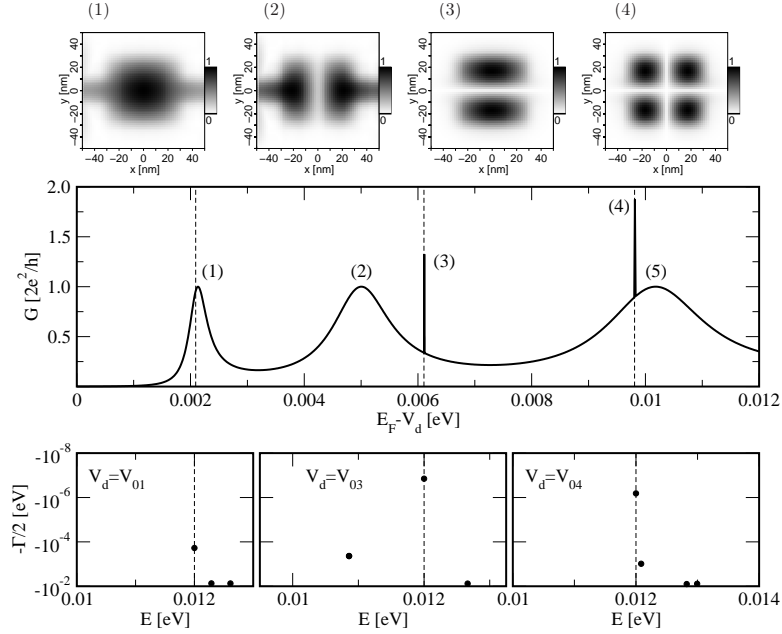


Figure 4: (Middle part) Conductance (solid line) as a function of the potential energy in the dot region, V_d . The vertical dashed lines give the position of the potential energy V_{0l} , $l = 1, 3, 4$. (Upper part) The space dependence of the electron probability distribution density $P_n(x, y)/P_{max}$, $P_n(x, y) = |\psi_n^{(s)}(E; x, y)|^2$, $P_{max} = \max[P_n(x, y)]$, $n = 1$ or $n = 2$, for $E = E_F$ and $V_d = V_{0l}$, $l = 1, 2, 3, 4$. For the peaks $l = 1, 2$ we have considered the channel number $n = 1$, while for the peaks $l = 3, 4$, $n = 2$. (Lower part) Resonance energies in the complex energy plane with the real part around E_F . The vertical dashed lines correspond to the Fermi energy.

But there is an exception which does not depend on the parameters of the system: the peak denoted by (6) in Fig. 5. Although the probability distribution density has a maximum in the central region of the dot, this state is strongly localized inside the dot, and the corresponding peak is very narrow. But this peak is not an asymmetric maximum anymore, it has a "S-type" Fano line shape. This behavior can be explained only taking into account the interaction between resonances. The state which corresponds to the peak (5) has three maxima in the x -direction and one maximum in the y -direction, while the peak (6) has one maximum on x - and three maxima on y -direction. They are states with the same symmetry in the both directions and they influence each other. As a result, there are two hybrid modes, one of them very strongly coupled to the contacts and the other one almost isolated. This interaction between resonant states with the same symmetry in the lateral direction is a general phenomenon which has at the origin the scattering between different energy channels due to the nonseparable character of the scattering potential. For systems with an effective 1D scattering potential the interaction between resonances is weak and the strong asymmetric Fano line shapes ("S-type" or antiresonance) do not appear. Also the hybrid modes do not exist in this case.

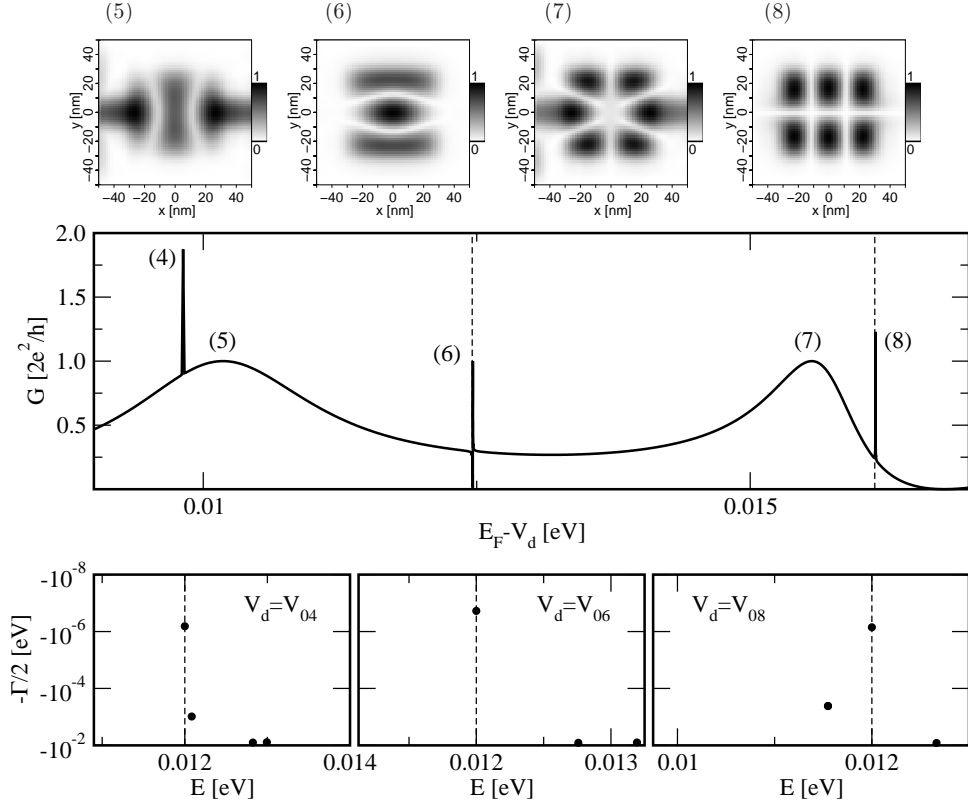


Figure 5: (Middle part) Conductance (solid line) as a function of the potential energy in the dot region, V_d . The vertical dashed lines give the position of the potential energy V_{0l} , $l = 6, 8$. (Upper part) The space dependence of the electron probability distribution density $P_n(x, y)/P_{max}$, $P_n(x, y) = |\psi_n^{(s)}(E; x, y)|^2$, $P_{max} = \max[P_n(x, y)]$ for $E = E_F$ and $V_d = V_{0l}$, $l = 5, 6, 7, 8$. For the peaks $l = 5, 6, 7$ we have considered the channel number $n = 1$, while for the peaks $l = 8$, $n = 2$. (Lower part) Resonance energies in the complex energy plane with the real part around E_F . The vertical dashed lines correspond to the Fermi energy.

Besides the potential energy in the dot region V_d , the confinement potential of the dot V_0 can be also modified by the top gates. Decreasing the strength of the confinement the coupling of the resonance states to the contacts increases, and the conductance peaks become broader. We present in Fig. 6 the evolution of the conductance peaks (7) and (8) when the potential V_0 decreases. The width of the two peaks increases, and the maximum of each peak migrates to higher energies. But the shift in energy is different. The state (7) which is strongly coupled to the contacts in the aperture regions is much less influenced by the variation of V_0 . The state which corresponds to the peak (8), with nearly zero probability distribution density in the region of the apertures, can have a coupling to the contacts only in the case of a rather transparent confinement barrier V_0 . This explains the significant broadening of the line shape and also the larger shift of the peak energy.

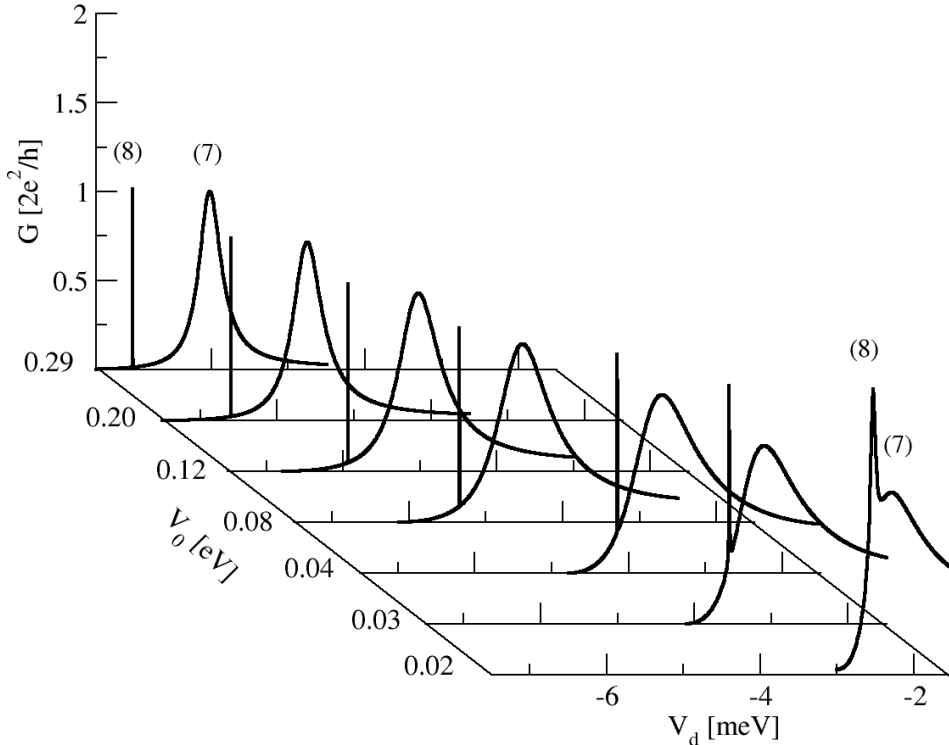


Figure 6: Conductance as a function of the potential energy in the dot region, V_d , for different values of the lateral confinement potential, V_0 .

3.2 Conical quantum dot inside a cylindrical nanowire

We consider a conical quantum dot, embedded in an infinite cylindrical nanowire with the same radius, as is sketched in Fig. 7(a). The parameters considered are the height of the dot $h = 5\text{nm}$, the radius of the nanowire $R = 5\text{nm}$ and the effective mass $m^* = 0.19m_0$. We set in our computations $d_{\parallel} = d_z = 16\text{nm}$ and the total number of channels (open and closed) $N = 8$. In our calculations, the results do not change if more channels are added.

Depending on the band-offsets between the dot material and the host material the potential produced by the dot can be repulsive, yielding a quantum barrier, or attractive, yielding a quantum well. We consider here that the dot yields an attractive potential $V(z, r)$, represented in Fig. 7(b) by a quantum well of depth $W_b = -0.125\text{eV}$.

The total tunneling coefficient $T^{(1)}$ versus the incident energy E is plotted in Fig. 8, for different magnetic quantum numbers m . The transmission increases with a unity, every time a new channel $E_{\perp, n}^{(m)}$ becomes available for transport, i.e. becomes open. The length of the plateaus is given by the difference between two successive transversal mode energies, and this length increases with m . Due to the presence of the quantum well, deviations appear from the step-like transmission. Just before

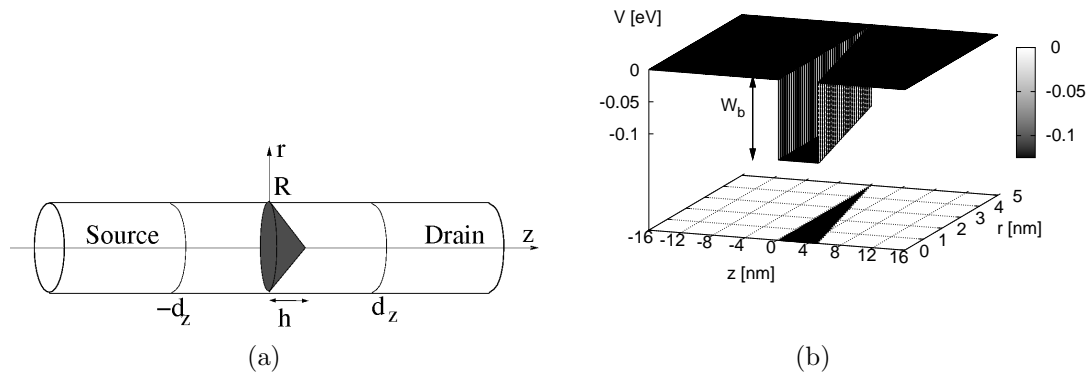


Figure 7: (a) Sketch of a conical quantum dot embedded into a nanowire with the same radius. The dot yields an attractive potential $V(z, r)$, represented in (b) by a quantum well of depth $W_b = -0.125\text{eV}$.

a new channel gets open there is a dip, i.e. sharp drop, in the tunneling coefficient. These dips are owing to modification of the tunneling coefficient due to the evanescent (closed) channels [33]. This is a multichannel effect that was also put in evidence in Cartesian coordinates for quantum wires tailored in a two-dimensional electron gas [33, 34, 35, 36, 37].

The dips can be understood considering the simple couple-mode model [33, 34, 35, 31]. For a dot surrounded by the host material, the scattering potential $V(z, r)$ is not anymore separable, so that the scattering mixes the channels [33, 34, 35, 31]. As soon as the scattering potential is attractive, the diagonal coupling matrix element

$$V_{nn}(z) = \int_0^R \phi_n(r)V(z, r)\phi_n(r)rdr < 0 \quad (52)$$

acts for every channel n as an effective one-dimensional (1D) attractive potential [34], which always allows for at least one bound state [46, 47] below the threshold of the continuum spectrum. By mixing the channels, this bound state becomes a *quasi-bound state* or resonance, i.e with complex energy, whose real part gets embedded into continuum spectrum of the lower channel and the imaginary part describes the width of the resonance. These resonances can be seen now as dips in the tunneling coefficient. The energy difference between the position of the dips and the next subband minima $E_{\perp, n}^{(m)}$ gives the quasi-bound state energy. The positions of the dips, i.e. the quasi-bound state energy, depend on the channel number n and on the magnetic quantum number m and, of course, on the detailed system parameters. In Cartesian coordinates the specific symmetry of the channels (odd and even) do not allow for dips in the first plateau [36]. In the cylindrical geometry this symmetry is broken, so that we obtain a dip in front of every plateau. Our numerical method allows for a high energy resolution in computing the tunneling coefficient, so that we were able to find the dips also in front of the higher-order plateaus.

Further insight about the quasi-bound states of the evanescent channels can be

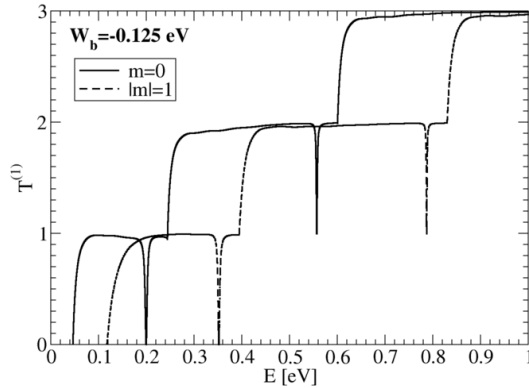


Figure 8: Total tunneling coefficient as a function of incident energy E for the scattering potential represented in Fig. 7(b) for different magnetic quantum numbers m (continuous line for $m = 0$, dashed line for $|m| = 1$) and for the well depth $W_b = -0.125\text{eV}$.

gained looking at the wave functions, whose square absolute value $|\psi_n^{(s)}(E; z, r)|^2$ gives the *localization probability distribution density*.

The R-matrix formalism allows us to produce high resolution maps of the wave functions inside the scattering region, see Eq. (33). In Figs. 9(a), 9(b) the localization probability distribution density is represented in arbitrary units, for an electron incident from source ($s = 1$) and with a total energy corresponding to the dips in Fig. 8. The total energy E and the channel n , on which the electron is incident, are specified at every plot. Let discuss Fig. 9(a). The total energy $E = 0.199\text{eV}$ is less than the energy of the second transversal mode, $E_{\perp,2}^{(0)} = 0.244\text{eV}$, so that only the first channel is open. Thus the incident wave from the source contact is node-less in r -direction. But, as it can be seen in Fig. 9(a), the scattering wave function inside the scattering region has a node in the r -direction, i.e. position in r where the wave function is zero. This means that the wave function corresponds to the quasi-bound state splitting off from the second transversal mode, which is an evanescent one. The quasi-bound state is reachable now in a scattering formulation due to channel mixing. The scattering wave function has a pronounced peak around the scattering potential, i.e. $z \in [0, 5]\text{nm}$, and decreases exponentially to the left and to the right. On the left side of the scattering potential one observes the interference pattern produced by the incident and the reflected waves, while on the right side there exists only the transmitted wave.

The scattering wave function considered in Fig. 9(b) has the energy less than the third transversal channel, $E_{\perp,3}^{(0)} = 0.6006\text{eV}$, so that the incident part of the scattering state on the second mode $n = 2$ has one node in r -direction. But the scattering function shows inside the scattering region two nodes in the r -direction, so it corresponds to a quasi-bound state splitting off from the above evanescent channel, the third one.

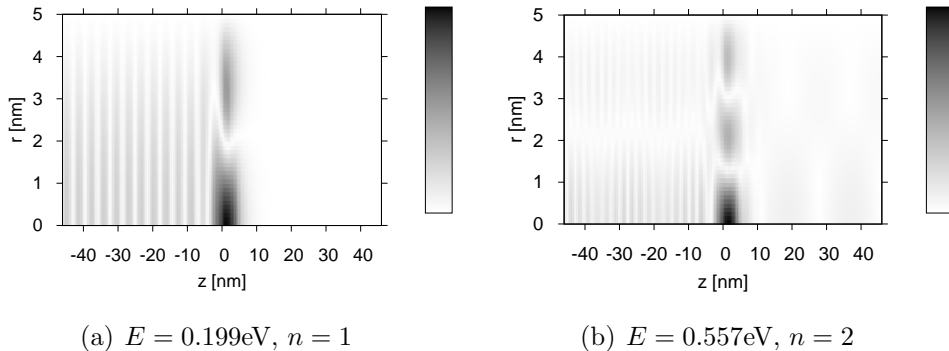


Figure 9: Localization probability distribution density, $|\psi_n^{(1)}(E; z, r)|^2$, for an electron with $m = 0$, incident from the reservoir $s = 1$ into the channel n and with the total energy E , both indicated in the captions. The energies are the dips in Fig. 8.

One gets similar pictures for all m -values, with the difference that for $m \neq 0$ the wave functions are zero for $r = 0$. In Fig. 9(a) and 9(b) one can observe that the transmitted part of the scattering wave function is zero, in agreement with the resonant back-scattering specific to the quasi-bound states of the evanescent channels [33, 34]. Increasing the strength of the attractive potential one can see more dips [36, 31] in the tunneling coefficient. Another systems embedded inside the cylindrical nanowire, like a cylindrical dot, a quantum ring or a double barrier heterostructure, which also show a similar behavior, were studied in Ref. [31].

We have analyzed until now only the classical allowed energy domain, with a continuous, double degenerated spectrum. The wave functions of the electrons for these energies are extended states, presented here as scattering states. The classically forbidden spectrum contains the bound states or the localized states. The R-matrix formalism presented here can provide also these states, as long as the boundary points $\pm d_z$ are far enough from the quantum dot, so that the bound states fulfill the Neumann boundary condition (28). In such a way, the energies of the bound states are the negative Wigner-Eisenbud energies and the wave functions for the bound state are the corresponding Wigner-Eisenbud functions. For the conical dot presented here, there is only a bound state represented by the lowest Wigner-Eisenbud energy, $E_b = E_1 < 0$ and $\psi_b(E_b; z, r) = \chi_1(z, r)$.

In Fig. 10(a) we present the energy value E_b of the bound state together with a cut of the potential energy along $r = 0$. The corresponding wave function, namely the absolute value square, is represented in Fig. 10(b). One can see that the bound state is mainly localized inside the quantum dot.

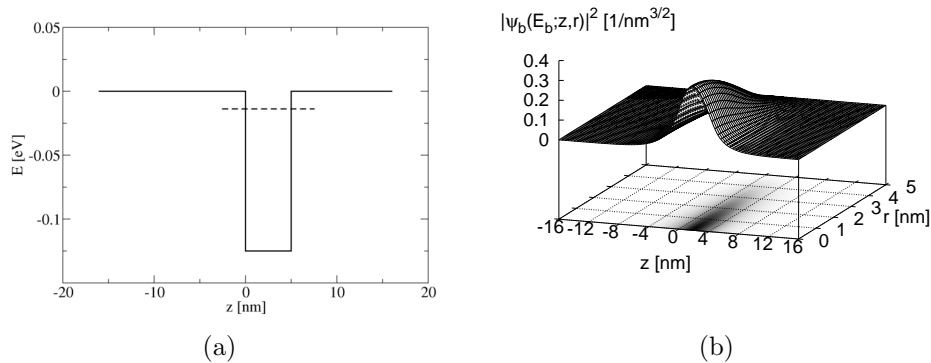


Figure 10: The bound state for a conical quantum dot inside the nanowire, as in Fig. 7. (a) Value of the bound energy $E_b = -0.013\text{eV}$ (dashed line). The potential energy along $r = 0$ is represented by the solid line. (b) The absolute value square of the wave function corresponding to the bound state, $|\psi_b(E_b; z, r)|^2$.

4 Summary and discussion

We have presented a general theory for computing the scattering matrix and the scattering wave functions for a general finite-range extended scattering potential in two dimensions. The theory is based on the R-matrix formalism, which allows a semi-analytical treatment of the scattering problem, yielding in such a way a powerful and efficient numerical method.

This formalism was applied to a quantum dot defined inside a two-dimensional electron gas, as well to a conical quantum dot embedded inside a cylindrical nanowire.

It is pointed out the role of the evanescent channels, which for a nonseparable attractive scattering potential in a multi-channel nanowire produces resonant dips in the tunneling coefficient. Furthermore, the cylindrical symmetry does not yield the same "selection rules" for tunneling coefficient as the Cartesian symmetry.

It is also presented a general resonance theory, which shows that the two-dimensional character of the scattering potential and the strong coupling of the quantum system to the contacts allow for the transmission profiles which ranges from asymmetric Fano line shapes through "S-type" Fano lines up to antiresonances.

Detailed maps of localization probability distribution density sustain the physical interpretation of the resonances (dips and peaks) found in the studied heterostructures.

Acknowledgment

It is a pleasure for us to acknowledge the fruitful discussions with Klaus Gärtner, Vidar Gudmundsson, Andrei Manolescu and Gheorghe Nenciu.

References

- [1] Semiconductor Industry Association, International Technology Roadmap for Semiconductors, <http://www.itrs.net>.
- [2] B. Doyle, R. Arghavani, D. Barlage, S. Datta, M. Doczy, J. Kavalieros, A. Murty, and R. Chau. *Intel Technology Journal*, 6:42–54, 2002.
- [3] T. Bryllert, L.-E. Wernersson, T. Loewgren, and L. Samuelson. Vertical wrap-gated nanowire transistors. *Nanotechnology*, 17:S227, 2006.
- [4] K. H. Yeo et al. Gate-All-Around (GAA) Twin Silicon Nanowire MOSFET (TSNWFET) with 15nm length gate and 4nm radius nanowire. *Tech. Dig. - Int. Electron Devices Meet.*, page 539, 2006.
- [5] K. H. Cho, K. H. Yeo, Y. Y. Yeoh, S. D. Suk, M. Li, J. M. Lee, M.-S. Kim, D.-W. Kim, D. Park, B. H. Hong, Y. C. Jung, and S. W. Hwang. Experimental evidence of ballistic transport in cylindrical gate-all-around twin silicon nanowire metal-oxide-semiconductor field-effect transistors. *Appl. Phys. Lett.*, 92:052102, 2008.
- [6] A. D. Wieck and K. Ploog. In-plane-gated quantum wire transistor fabricated with directly written focused ion beams. *Appl. Phys. Lett.*, 56:928–930, 1990.
- [7] J. Göres, D. Goldhaber-Gordon, S. Heemeyer, M. A. Kastner, H. Shtrikman, D. Mahalu, and U. Meirav. *Phys. Rev. B*, 62:2188, 2000.
- [8] H.-S.P. Wong, K.K. Chan, and Y. Taur. Self-aligned (top and bottom) double-gate mosfet with a 25 nm thick silicon channel. *IEDM Tech. Dig.*, pages 427–430, 1997.
- [9] X. Huang, W.-C. Lee, C. Kuo, D. Hisamoto, L. Chang, J. Kedzierski, E. Anderson, H. Takeuchi, Y.-K. Choi, K. Asano, V. Subramanian, T.-J. King, J. Bokor, and C. Hu. Sub 50-nm finfet: Pmos. *IEDM Tech. Dig.*, pages 67–70, 1999.
- [10] B.S. Doyle, S. Datta, M. Doczy, S. Harelund, B. Jin, J. Kavalieros, T. Linton, A. Murthy, R. Rios, and R. Chau. High performance fully-depleted tri-gate cmos transistors. *IEEE Electron Dev. Lett.*, 24:263–265, 2003.
- [11] J. Xiang, W. Lu, Y. Hu, Y. Hu, H. Yan, and C. M. Lieber. Ge/Si nanowire heterostructures as high-performance field-effect transistors. *Nature*, 441:489, 2006.
- [12] M.T.Bjork, B.J.Ohlsson, C. Thelander, A.I. Persson, K. Deppert, L.R. Wallenberg, and L. Samuelson. Nanowire resonant tunneling diodes. *Appl. Phys. Lett.*, 81:4458, 2002.

- [13] J. Wensorra, K. M. Indlekofer, M. I. Lepsa, A. Forster, and H. Lüth. Resonant tunneling in nanocolumns improved by quantum collimation. *Nano Lett.*, 5:2470, 2005.
- [14] F. Qian, Y. Li, S. Gradec Caronak, H.-G. Park, Y. Dong, Y. Ding, Z. L. Wang, and C. M. Lieber. Multi-quantum-well nanowire heterostructures for wavelength-controlled lasers. *Nature Mater.*, 7:701, 2008.
- [15] Y. Hu, H. O. H. Churchill, D. J. Reilly, J. Xiang, C. M. Lieber, and C. M. Marcus. A Ge/Si heterostructure nanowire-based double quantum dot with integrated charge sensor. *Nature Nanotechnol.*, 2:622, 2007.
- [16] B. Tian, X. Zheng, T. J. Kempa, Y. Fang, N. Yu, G. Yu, J. Huang, and C. M. Lieber. Coaxial silicon nanowires as solar cells and nanoelectronic power sources. *Nature*, 449:885, 2007.
- [17] K. H. Cho et al. Observation of single electron tunneling and ballistic transport in Twin Silicon Nanowire MOSFETs (TSNWFETs) fabricated by top-down CMOS Process. *Tech. Dig. - Int. Electron Devices Meet.*, page 543, 2006.
- [18] D. Vasileska, D. Mamaluy, H. R. Khan, K. Ravela, and S. M. Goodnick. Semiconductor Device Modeling. *J. Comput. Theor. Nanosci.*, 5:999–1030, 2008.
- [19] L. Smrčka. R-matrix and the coherent transport in mesoscopic systems. *Superlatt. and Microstruct.*, 8:221, 1990.
- [20] U. Wulf, J. Kučera, P. N. Racec, and E. Sigmund. Transport through quantum systems in the R-matrix formalism. *Phys. Rev. B*, 58:16209, 1998.
- [21] E. Onac, J. Kučera, and U. Wulf. Vertical magnetotransport through a quantum dot in the R-matrix formalism. *Phys. Rev. B*, 63:85319, 2001.
- [22] E. R. Racec and U. Wulf. Resonant quantum transport in semiconductor nanostructures. *Phys. Rev. B*, 64:115318, 2001.
- [23] P. N. Racec, E. R. Racec, and U. Wulf. Capacitance in open quantum structures. *Phys. Rev. B*, 65:193314, 2002.
- [24] G. A. Nemnes, U. Wulf, and P. N. Racec. Nano-transistors in the Landauer-Büttiker formalism. *J. Appl. Phys.*, 96:596, 2004.
- [25] G. A. Nemnes, U. Wulf, and P. N. Racec. Non-linear I-V characteristics of nano-transistors in the Landauer-Büttiker formalism. *J. Appl. Phys.*, 98:084308, 2005.
- [26] T. Jayasekera, M. A. Morrison, and K. Mullen. R-matrix theory for magnetotransport properties in semiconductor devices. *Phys. Rev. B*, 74:235308, 2006.
- [27] U. Wulf, P. N. Racec, and E. R. Racec. Admittance of planar two-terminal quantum systems. *Phys. Rev. B*, 75:075320, 2007.

- [28] J. Behrndt, H. Neidhardt, E. R. Racec, P. N. Racec, and U. Wulf. On Eisenbud's and Wigner's R-matrix: A general approach. *J. Differ. Equ.*, 244:2545, 2008.
- [29] G. Mil'nikov, N. Mori, and Y. Kamakura. R-matrix method for quantum transport simulations in discrete systems. *Phys. Rev. B*, 79:235337, 2009.
- [30] E. P. Wigner and L. Eisenbud. Higher angular momenta and long range interaction in resonance reactions. *Phys. Rev.*, 72:29, 1947.
- [31] P. N. Racec, E. R. Racec, and H. Neidhardt. Evanescent channels and scattering in cylindrical nanowire heterostructures. *Phys. Rev. B*, 79:155305, 2009.
- [32] E. R. Racec, P. N. Racec, and U. Wulf. unpublished.
- [33] Philip F. Bagwell. Evanescent modes and scattering in quasi-one-dimensional wires. *Phys. Rev. B*, 41:10354–10371, 1990.
- [34] S. A. Gurvitz and Y. B. Levinson. Resonant reflection and transmission in a conducting channel with a single impurity. *Phys. Rev. B*, 47:10578–10587, 1993.
- [35] Jens U. Nöckel and A. Douglas Stone. Resonance line shapes in quasi-one-dimensional scattering. *Phys. Rev. B*, 50:17415–17432, 1994.
- [36] J. H. Bardarson, I. Magnusdottir, G. Gudmundsdottir, C.-S. Tang, A. Manolescu, and V. Gudmundsson. Coherent electronic transport in a multi-mode quantum channel with gaussian-type scatterers. *Phys. Rev. B*, 70:245308, 2004.
- [37] V. Gudmundsson, Y.-Y. Lin, C.-S. Tang, V. Moldoveanu, J. H. Bardarson, and A. Manolescu. *Phys. Rev. B*, 71:235302, 2005.
- [38] Bastard G., Brum J. A., and Ferreira R. *Sol. State Phys.*, 44:229, 1991.
- [39] F. F. Fang and W. E. Howard. Negative field-effect mobility on (100) si surfaces. *Phys. Rev. Lett.*, 16:797–799, 1966.
- [40] M. Baro, H.-Ch. Kaiser., H. Neidhardt, and J. Rehberg. A quantum transmitting Schrödinger-Poisson system. *Rev. Math. Phys.*, 16:281–330, 2004.
- [41] H Schanz and U. Smilansky. Quantization of sinais billiard - a scattering approach. *Chaos Solitons & Fractals*, 5:1289–1309, 1995.
- [42] M. Luisier, A. Schenk, and W. Fichtner. Quantum transport in two- and three-dimensional nanoscale transistors: Coupled mode effects in the nonequilibrium Green's function formalism. *J. Appl. Phys.*, 100:043713, 2006.
- [43] A. M. Lane and R. G. Thomas. R-matrix theory of nuclear reactions. *Rev. Mod. Phys.*, 30:257, 1958.

- [44] M. Büttiker, Y. Imry, R. Landauer, and S. Pinhas. Generalized many-channel conductance formula with application to small rings. *Phys. Rev. B*, 31:6207, 1985.
- [45] A. Bohm. *Quantum Mechanics*. Springer, New York, 1993.
- [46] B. Simon. The bound state of weakly coupled Schrödinger operators in one and two dimensions. *Ann. Physics*, 97:279, 1976.
- [47] M. Klaus. On the bound state of Schrödinger operators in one dimension. *Ann. Physics*, 108:288, 1977.